YALE PEABODY MUSEUM

Journal of Marine Research

The *Journal of Marine Research,* one of the oldest journals in American marine science, published important peer-reviewed original research on a broad array of topics in physical, biological, and chemical oceanography vital to the academic oceanographic community in the long and rich tradition of the Sears Foundation for Marine Research at Yale University.

An archive of all issues from 1937 to 2021 (Volume 1–79) are available through EliScholar, a digital platform for scholarly publishing provided by Yale University Library at https://elischolar.library.yale.edu/.

Requests for permission to clear rights for use of this content should be directed to the authors, their estates, or other representatives. The *Journal of Marine Research* has no contact information beyond the affiliations listed in the published articles. We ask that you provide attribution to the *Journal of Marine Research.*

Yale University provides access to these materials for educational and research purposes only. Copyright or other proprietary rights to content contained in this document may be held by individuals or entities other than, or in addition to, Yale University. You are solely responsible for determining the ownership of the copyright, and for obtaining permission for your intended use. Yale University makes no warranty that your distribution, reproduction, or other use of these materials will not infringe the rights of third parties.

Winter conditions in the Irminger Sea observed with profiling floats

by L. R. Centurioni[1] and W. J. Gould[1]

ABSTRACT

Temperature/salinity profiles collected between 1994 and 2003 with profiling floats in the North Atlantic subpolar gyre are analyzed to investigate the hydrographic conditions in winter in the Irminger Sea. The salinity data can be calibrated against accurate profiles from ships obtained mostly during summer months and the resulting float profile salinity accuracy is of the order of 0.015. Between 1997 and 2003, when the North Atlantic Oscillation (NAO) index was generally low, the potential temperature and salinity of the Labrador Sea Water (LSW) core observed by the floats showed a positive trend, an indication of little or no deep convection. The float data show that in the Irminger Sea the thermal energy of the water column reaches the lowest values south and southwest of Cape Farewell, a place where deep convective events are likely to occur. The geostrophic velocity field at 15 m computed from drifting buoys and satellite measurements of sea level shows, for the same area, mean currents below 0.1 m s^{-1} and low levels of eddy kinetic energy. These factors, together with recent estimates of winter air-sea heat fluxes as high as 500 W m^{-2} for this region, are exploited to explore the evolution of the surface mixed layer using several one-dimensional models. The results suggest that the typical thickness of the surface mixed layer at the end of winter is of the order of 400 m. This is similar to observed values from floats.

1. Introduction

In this work we analyze salinity-temperature-depth profiles collected between November 1994 and June 2003 with autonomous profiling floats (Davis *et al.,* 1992; Davis, 1998) to investigate the physical characteristics of the water masses in part of the North Atlantic subpolar gyre. The focus is on the interior of the Irminger Sea in winter months, a place where intense cooling of the upper ocean takes place through the atmosphere-ocean interface. The float data represent a unique resource to study the hydrography of this region in winter. The purpose of this research is to show that accurate measurements can be obtained, after a careful calibration of the salinity data, using Argo (Roemmich *et al.,* 2001), a pre-operational ocean observing system, and that those data can be used to identify the region where the deepest winter mixed layers are most likely to occur. The data from another ocean observing system, the array of Surface Velocity Program (SVP)

1. Scripps Institution of Oceanography, University of California, 9500 Gilman Drive, La Jolla, California, 92093-0213, U.S.A. *email: lcenturioni@ucsd.edu*
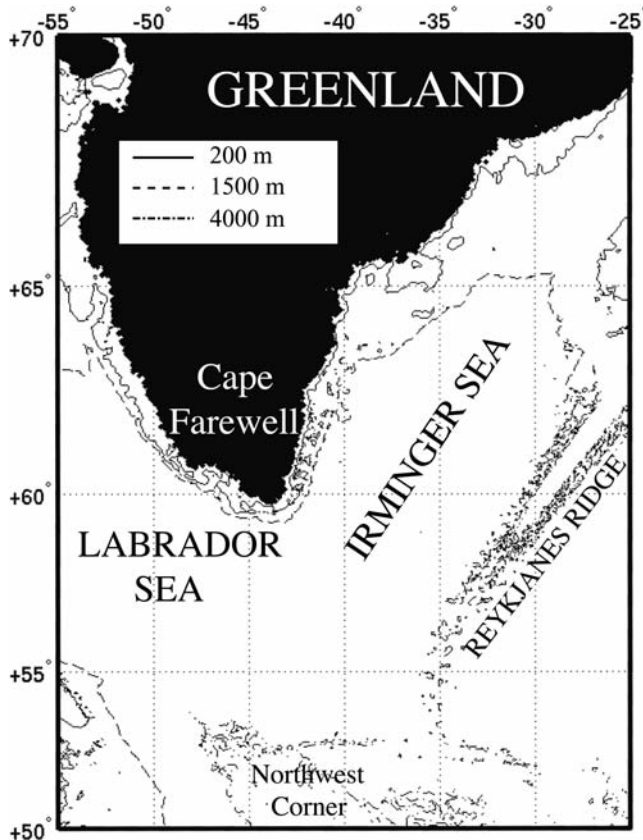
Figure 1. Bathymetry of the study region (Smith and Sandwell (1997), bathymetry version 8.2). Mercator projection.

drifters (Niiler, 2001) combined with Mean Surface Level Anomalies (MSLA) measurements from satellites, are also exploited to compute the mean near-surface geostrophic velocity field of the Irminger Sea and adjacent regions.

The mean circulation in the Irminger Sea (see Fig. 1 for a map of the region), at least in the upper 700 m, is cyclonic. This has been documented at the surface with drifters drogued at 15 m (Fratantoni, 2001; Reverdin *et al.,* 2003) and at 700 m with profiling floats (Lavender *et al.,* 2000). The water mass distribution obtained from hydrographic observations (see for example Bersch *et al.,* 1999) reflects these circulation patterns. The basin-scale circulation is driven by a local, seasonally varying, positive wind stress curl that reaches maximum intensity in February (Spall and Pickart, 2003). Generally weak stratification and the presence of steeply sloping boundaries set the vertical scale of the circulation to a value much larger than the mean depth of the basin and support the existence of slow phase speed topographic Rossby waves that maintain the circulation in

an approximately steady state (Spall and Pickart, 2003). The generally cyclonic circulation in the Irminger Sea induces upward doming of the isopycnal surfaces, implying that the domed region is where water mass transformation can occur most easily, provided that buoyancy fluxes are large enough to produce convective overturning to sufficient depth (Pickart *et al.,* 2003a).

On the western side of the Reykjanes Ridge, the mean flow, both at the surface and at greater depths, is toward the northeast and, at least near the surface, forms a continuous current system usually identified as the Irminger Current, which transports salty and warm (compared to the interior of the basin) Modified North Atlantic Water (MNAW) cyclonically around the basin. (See for example Krauss, 1995). The distribution, temperature and salinity of MNAW in the Irminger Sea are subject to significant seasonal and interannual changes (Mortensen and Valdimarsson, 1999). Part of this circulation of MNAW leaves the Irminger Sea by flowing north through the Denmark Strait and part recirculates southwestward along the coast of Greenland (Orvik and Niiler, 2002). While flowing southwestward, the Irminger Current forms a sharp thermal front with the much cooler and fresher East Greenland Current (and farther inshore the East Greenland Coastal Current; Bacon *et al.,* 2002) that transport Polar Surface Water above the continental shelf and slope and enter the Irminger Sea through the western side of the Denmark Strait. The current system formed by the East Greenland Current, the Irminger Current and the East Greenland Coastal Current shows two speed maxima at the surface (see for example Reverdin *et al.,* 2003) and, on average, these jets exhibit mean speeds of about 0.3 m s^{-1} (Bruce, 1995). At the front between the East Greenland Current and the Irminger Current, eddies with a diameter of some 20 to 40 km develop and are advected to the southwest (Bruce, 1995; Krauss, 1996; Eden and Böning, 2002). Larger eddies, some 70 km in diameter, are also observed in the interior of the basin (Krauss, 1995). On the East Greenland continental slope the Irminger Current is underlain by Denmark Strait Overflow Water, usually deeper than 800 m south of the Denmark Strait sill (Rudels *et al.,* 1999) and with peak speeds of about 1 m s^{-1} (Dickson *et al.,* 1990) to 1.5 m s^{-1} (Bruce, 1995) when an eddy is present.

High values of surface eddy kinetic energy are observed in the boundary current system over the Greenland continental shelf in both the Irminger and the Labrador seas (Fratantoni, 2001; Reverdin *et al.,* 2003; Eden and Böning, 2002). In the Labrador Sea, the area of high eddy kinetic energy extends from the shelf region toward the middle of the basin at about 61N and there the associated eddy fluxes are thought to enhance the restratification process (Eden and Böning 2002; Katsman *et al.,* 2004) after intense winter cooling has overturned and homogenized the water masses in the central Labrador Sea to generate Labrador Sea Water (LSW, e.g. Talley and McCartney, 1982; Clarke and Gascard, 1983; Dickson *et al.,* 1996; Lavender *et al.,* 2000).

The Labrador Sea Water is found in the Irminger Sea typically below 1000 m (see e.g. Talley and McCartney, 1982). Until a few years ago, the Labrador Sea was regarded as the only site of the formation of LSW. Sy *et al.* (1997) estimated a transit time of six months for this water mass to reach the Irminger Basin from the Labrador Sea. Significantly longer

transit times, up to four times longer, were estimated from numerical simulations (Pickart *et al.,* 2003b; Straneo *et al.,* 2003). These and other recent studies have revisited the idea (Sverdrup *et al.,* 1942) that Labrador Sea Water can also be formed in the Irminger Sea, a place where heat fluxes from the ocean to the atmosphere can have peak values larger than 500 W m^{-2} (see also Pickart *et al.* (2003b) for a review on the subject). The process of densification of the upper water of the Irminger Sea is thought to be most likely beneath the path of a localized and intermittent meteorological phenomenon, the Greenland tip jet, which funnels air from the landmass and sustains heat fluxes comparable to those measured in the Labrador Sea in winter (Doyle and Shapiro, 1999; Pickart *et al.,* 2003a). Furthermore, the cooling of the sea surface by the Greenland tip jet is thought to be particularly effective in deepening the surface mixed layer since this wind blows over an area that includes the southern end of a cyclonic recirculation cell in the eastern Irminger Sea (Lavender *et al.,* 2000; Spall and Pickart, 2003). In the center of this domed gyre, where the mean velocity field is weak, Pickart *et al.* (2003a) postulated the potential to form surface mixed layers to depths in excess of 2000 m based on results from a regional oceanic model forced with an idealized wind that simulates the Greenland tip jet. Deep convection events are known to produce uniform water masses from the surface to about 2000 m in the Labrador Sea with potential density uniform within 0.01 kg m^{-3} (Clarke and Gascard, 1983). Events of that magnitude have never been observed in the Irminger Sea. This may be because until now there have been almost no winter-time hydrographic observations in the area.

The production of LSW is highly variable and consequently the characteristic potential temperature and salinity of this water mass also vary as well (Talley and McCartney, 1982; Dickson *et al.,* 1996). The distribution of LSW in the subpolar gyre can be mapped by its potential vorticity (Talley and McCartney, 1982, their Fig. 3) and Pickart *et al.,* 2003a,b). Talley and McCartney, using data from a moderate to low NAO period (1950s/60s), show that the most recently ventilated water, characterized by a potential vorticity lower than $4 \cdot 10^{-12}$ m^{-1} s^{-1} fills the Labrador Sea and the central south western Irminger Sea, being confined, in the latter, south of 58N and west of 41W, while values between 4 and $8 \cdot 10^{-12}$ m^{-1} s^{-1} are found elsewhere in the Irminger Sea as far north as ~65.5N. At this northern latitude the likelihood of significant deep overturning activity is much reduced due to the combined effect of the buoyant surface layer of warm, although salty, MNAW and less severe meteorological forcing compared to the southwestern sector. However, Pickart *et al.* (2003b), analyzed CTD cruise data from a recent high NAO period, (1990–1997) in which convection was active in the western N. Atlantic. They showed a separate, low PV area in the SW Irminger Sea. The rate of production of LSW, the location of convection sites and the characteristic potential temperature and salinity of this water mass all vary from year to year (Talley and McCartney, 1982; Dickson *et al.,* 1996).

In Section 2 we present the data sets used in this study and outline the procedures used to calibrate the salinity data from the floats. A brief description of our estimate of the surface velocity field of this region using data from August 1990 to May 2002 is also given. The

results, presented in Section 3, are used to identify the portion of the Irminger Sea where the deepest mixed layers are most likely to occur. The identification of this area is based on the criteria of weak mean flow and deep mixed layers from floats. The likelihood of deep mixed layers is analyzed by applying several one-dimensional models of deep convection to predict the depth of the mixed layers at the end of winter. This is done in Section 4 where a discussion of the results are also given.

2. Data and methods

Commencing in 1994 neutrally buoyant profiling floats (Profiling Autonomous Lagrangian Circulation Explorer, PALACE) were deployed in the subpolar gyre as part of the World Ocean Circulation Experiment (WOCE) and more floats of newer design (Provor and Apex) were deployed from 2000 onward by the Argo program (Roemmich *et al.*, 2001). Most of the early floats had only pressure and temperature sensors but gradually conductivity (salinity) cells were added. The data set analyzed in this study was obtained by merging the WOCE profiling float data (WOCE Data Products Committee 2002) with the more recent Argo data (available online at: *http://www.usgodae.org/argo/argo.html;* see Table 1 in the Appendix for a list of World Meteorological Organization IDs of the instruments used for this study). The final data set consists of 3137 temperature-only profiles and 4587 temperature/salinity profiles contained in the box 50–66N and 50–25W and taken between November 1994 and June 2003 (Fig. 2). Most profiles were taken after 1997. Sixty-seven percent of the profiles penetrate deeper than 1200 dbar. The temperature and pressure data were assumed to fall within the sensor's specifications that typically are of the order of 0.002°C for the accuracy and 0.0005°C year^{-1} for the drift (Wong *et al.*, 2003) and thus to be free from significant errors for this study, the salinity data need calibration. Here it is assumed that the salinity error can be considered as a constant offset (Bacon *et al.*, 2001; Wong *et al.*, 2003). The calibration was performed by direct comparison, in the potential temperature (θ)-salinity (S) space, of deep portions (typically below 1000 dbar) of S-profiles from floats with the very accurate S profiles taken from ships. While the float data are collected year-round, the ship-based CTDs were mostly collected in the summer months (Table 2 in Appendix) and none of the ship-based observations was taken between December and March. A mean depth-independent offset was computed for each float profile (see Bacon *et al.* (2001) for a more detailed description of the method).

For this study, given the large number of profile data, we computed the reference salinity profiles by objectively mapping to each location of the float the accurate profile data from ships available in the Irminger Sea since 1990 (see Wong *et al.* (2003) for a description of the technique). The working area for the calibration and, therefore, the reference data set for the salinity, was taken inside an area with borders some 20 nautical miles offshore from the 1500 m bathymetry line (as given by the Smith and Sandwell (1997) bathymetry, see Fig. 3). The reference data set consisted of 457 Conductivity-Temperature-Depth (CTD) stations occupied by research vessels (see Table 2 in the Appendix for a list of the cruise data used for this research).
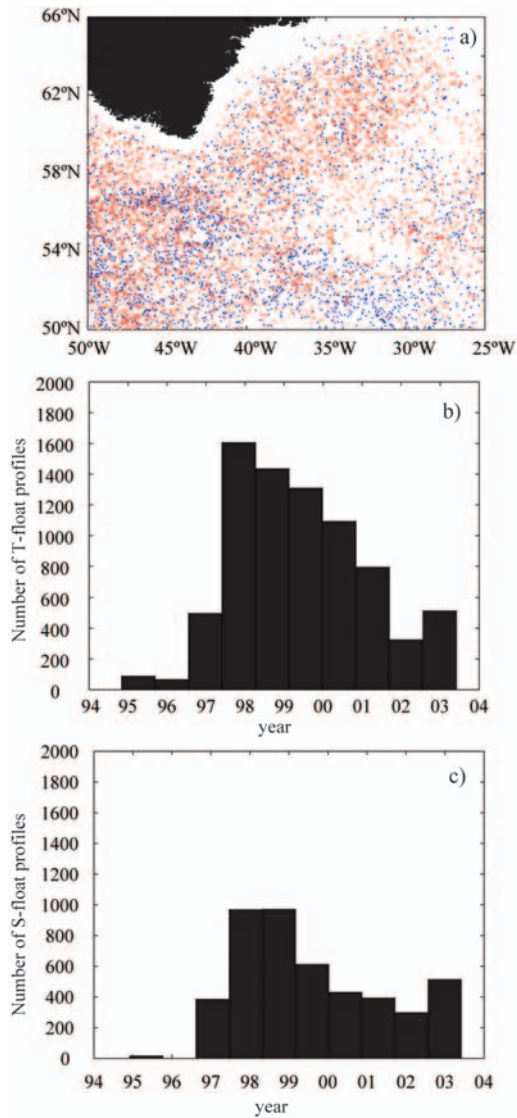
Figure 2. (a) Location of temperature-only profiles (blue) and temperature-salinity profiles (red) measured by the floats. (b) Time distribution of temperature profiles from floats. The total number of temperature profiles is 7725, taken between November 1994 and June 2003. (c) Time distribution of salinity profiles from floats. The total number of salinity profiles is 4587, taken between December 1994 and June 2003.

The salinity mapping function that best fitted the observations has the form $\exp(-(L/L_0)^{1/2})$. The de-correlation length scale L_0 (first zero crossing) for the salinity was estimated from the ship data θ-S curve computed by restricting the depth range between 1100 and
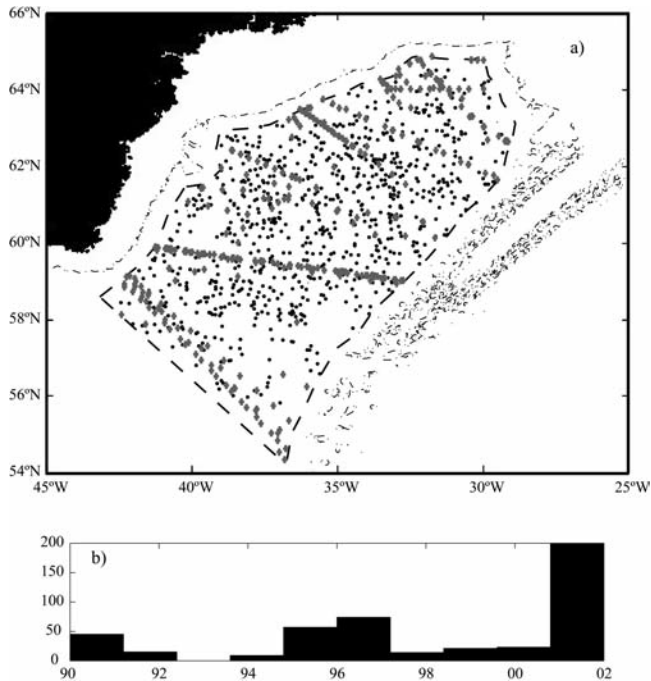
Figure 3. (a) Location of temperature and salinity profiles (1360) measured from floats (black dots) for which the calibration was performed. The figure also shows the position of the temperature and salinity profiles (457) measured from ships (grey crosses) that were for float calibration. The 1500 m depth contour is shown with a thin black line. The thick dashed black line encompasses a region with boundaries at a distance of some 20 nm from the 1500 bathymetry line. (b) Time distribution of temperature and salinity profiles taken from ships. None of these observations was made between January and March.

1500 dbar and by averaging the salinity into 0.05°C θ bins, with θ ranging from 2.5°C to 4°C. The salinity de-correlation length scale for the Irminger Sea was estimated at 18 km. This value is most likely biased low because it also reflects temporal changes of the θ-S properties of the water masses in this depth range, which are known to exist (Bersch *et al.*, 1999). The time scale for the objective mapping was arbitrarily set to 45 days (a seasonal timescale). The depth-independent mean salinity offset was computed for groups of three to five contiguous float profiles measured by the same instrument (one or two profiles taken before and one or two profiles taken after the one under examination) and the error of the offset was computed from standard formulae of error propagation. Profiles with a salinity offset larger than 0.2 were discarded. Figure 4 shows the θ-S diagram of measurements from floats before and after the calibration. The estimated median accuracy of the calibrated salinity measurements is approximately 0.015. The banded structure is due to some floats only measuring salinity with a resolution of 0.01.

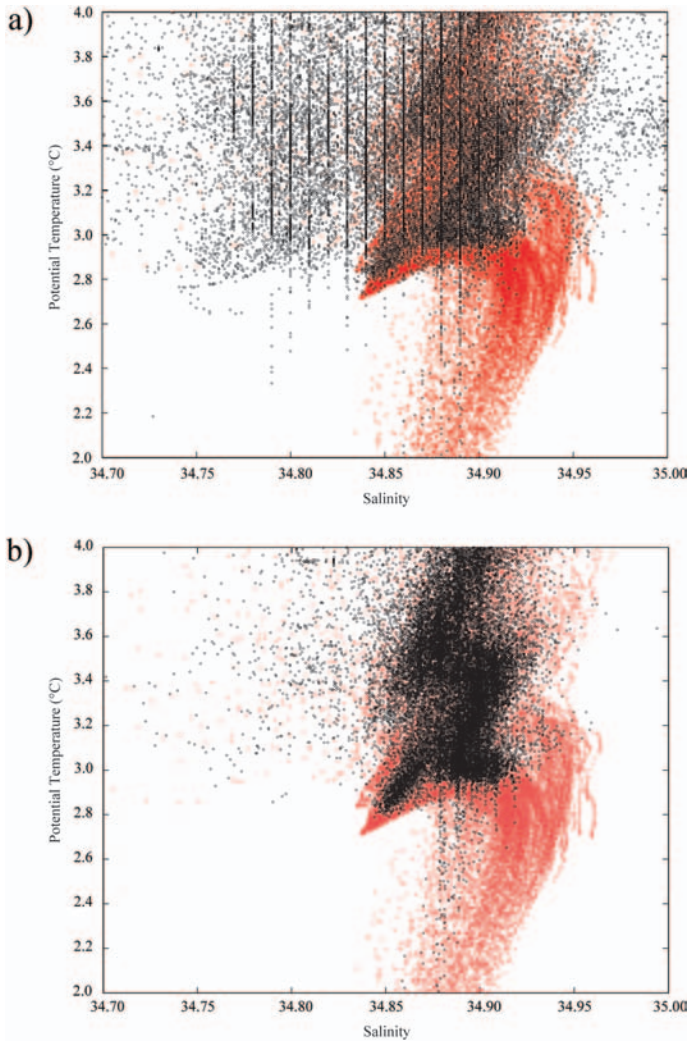The potential temperature profiles (although computed for simplicity using uncalibrated

Figure 4. (a) θ-*S* diagram from float data (black). The float salinity data are uncalibrated. The reference curves obtained from accurate θ-*S* measurements from ships are shown in red. (b) As in (a) but now with calibrated float salinity data. This figure also shows the cold (2.75–3.15°C) and fresh (34.84–34.91) signature of the Labrador Sea Water.

salinities following a visual check to eliminate obviously erroneous profiles) were interpolated at 10 dbar intervals and used to compute the thermal energy per unit area, defined as

$$E = \int_{z(\theta_{ref})}^{0} \rho_0(S, T) c_{p,0}(S, \theta) \theta(S, z') dz', \tag{1}$$
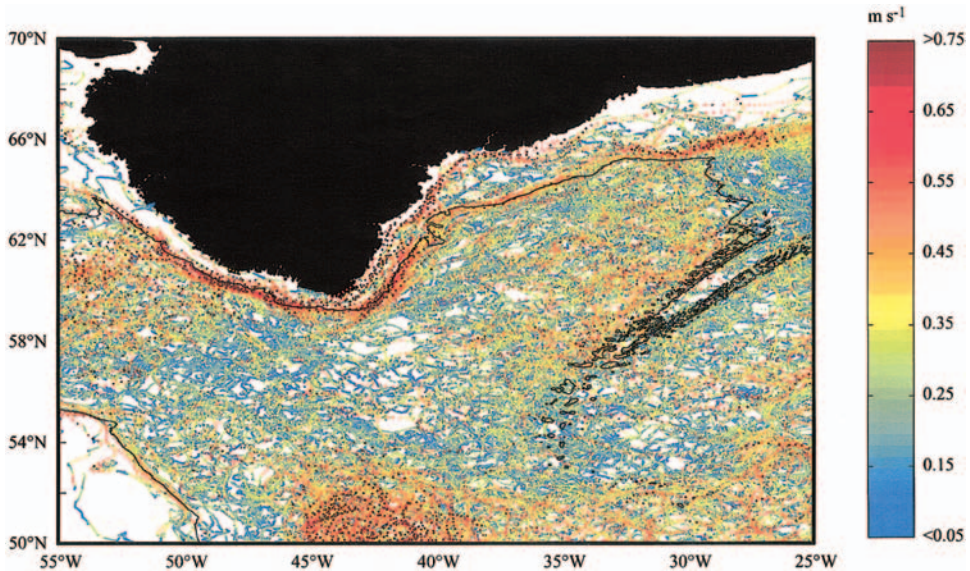
Figure 5. Six hourly position of 303 SVP drifters color coded in accordance with their instantaneous
   speed. 196413 measurements are shown, taken between 06 August 1990 and 30 June 2003. The
   black line represents the 1500 m bathymetry contour.

where ρ_0 is the water density referenced to the surface and $c_{p,0}$ is the specific heat at constant pressure referenced to the surface, and z is the water depth. The water depth was considered equivalent to the pressure. Eq. 1 was computed from the pressure $p(\theta_{ref})$ of the reference isotherm θ_{ref}. The reference pressure was approximated, for each profile, with the deepest level for which $3.3°C < \theta < 3.4°C$, yielding a median value for θ of $3.305°C$ over the whole domain. Furthermore, to identify possible sites of deep convection in the Irminger Sea and in adjacent areas the 1-D mixed layer model described by Clarke and Gascard (1983), with the lateral mixing algorithm removed and ignoring evaporation, was applied to the θ and S float profiles taken between January and the first week of April to compute the amount of heat transfer needed to achieve a mixed layer depth of 1000 dbar everywhere.

The near-surface geostrophic currents can be computed from drifter data by removing the Ekman component due to the wind (Ralph and Niiler, 1999). This operation offers a means of comparing this relatively sparse but directly-measured data set with measurements of MSLA measurements from satellites (Aviso data set). The latter data set can, therefore, be calibrated against the former and an estimate of the unbiased mean geostrophic velocity at 15 m can then be obtained (Niiler *et al.,* 2003). The Surface Velocity Program (SVP) drifter data set (Niiler, 2001) included, in the box bounded by 50N/70N and 55W/25W, 196413 six-hourly velocity measurements at 15 m depth taken, between 6 August 1990 and 30 June 2003, by 303 SVP buoys (Fig. 5). The unbiased
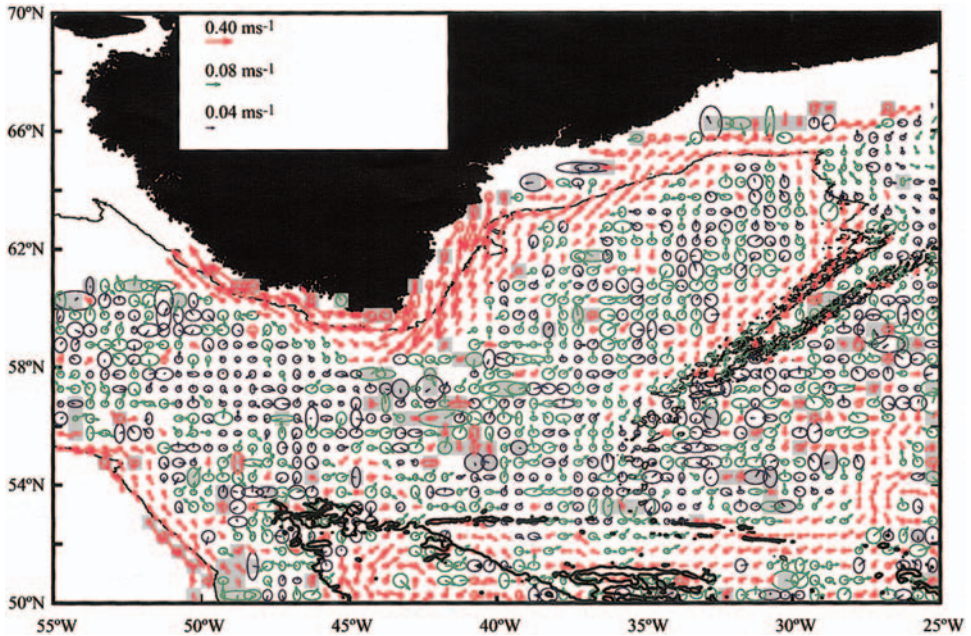
Figure 6. Unbiased mean geostrophic velocity field and standard error ellipses at 15 m computed at a resolution of 0.5° × 0.5° from drifters velocity measurements and MSLA altimetry data from satellites. The computation was performed over 31770 velocity measurements resulting from the application of a modified Hanning filter and 3.5 days time averaging to the original data set of 196413 velocity observations (see Fig. 5). The thin (thick) black line represents the 1500 (4000) m depth contour. Grey cells contain less (more) than 10 (5) observations. Velocity vectors in cells with less than five observations are not shown.

velocity field (Niiler *et al.,* 2003) and its standard error, that is the standard error of the intercept of this linear model, was computed at a resolution of 0.5° × 0.5°, after the application of a two-inertial period Hanning filter and a two-day averaging window.

3. Summary of observations

Instantaneous speeds at 15 m depth larger than 0.4 m s^{-1} were often measured close to the 1500 m contour and on the continental shelf along the coast of Greenland, in the Labrador Sea and along the northwestern side of the Reykjanes Ridge in the Irminger Sea (Fig. 5). South of approximately 53N (and south of 58N east of 29W) the high speeds associated with the North Atlantic Current can be seen. The region south of Cape Farewell has very few velocity observations. The unbiased mean geostrophic velocity field at 15 m (Fig. 6) reveals the structure of the East and West Greenland boundary currents, a northward flowing branch of the North Atlantic Current at about 33W and a well defined mean current around the Reykjanes Ridge that begins near the southwest tip of the ridge,
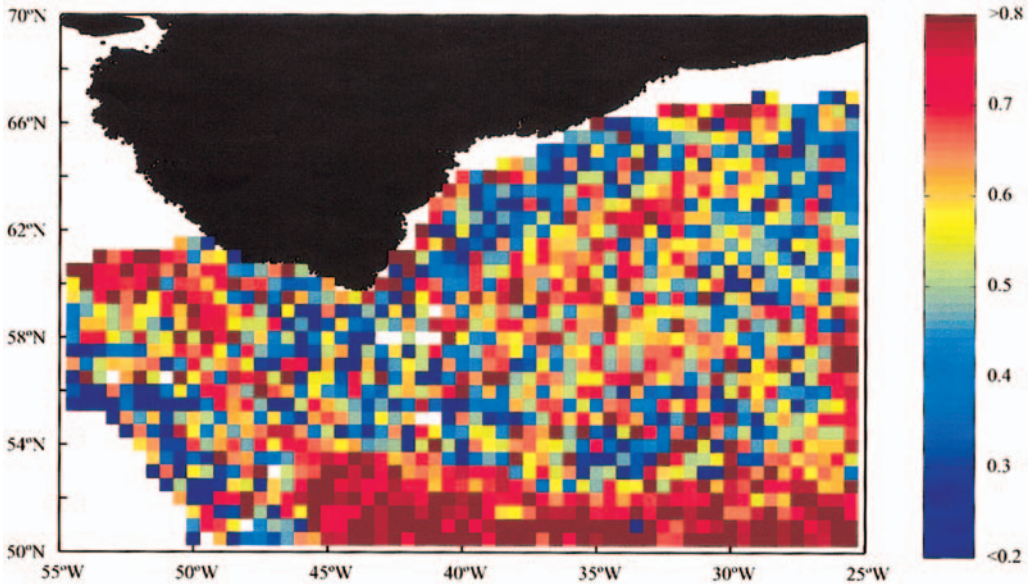
Figure 7. Correlation coefficient (on a 0.5° × 0.5° grid) between geostrophic velocity residuals estimated from drifter and from satellite measurements.

and flows northeastward, on the northwestern flank, to form the warm and salty Irminger Current. A mean northward flow weaker than 0.08 m s^{-1} is found south of 58N between 35W and 40W. The regions with the weakest mean flow are the interior of the Irminger and Labrador seas. In the northwest corner region the surface flow is similar to the one observed at greater depths (Zhang *et al.,* 2001). The correlation coefficient (Fig. 7) between the geostrophic current anomalies computed from the satellite altimetry data and the geostrophic current anomalies computed from the drifters (Niiler *et al.,* 2003) is generally greater than 0.6 in the interior of the Labrador and Irminger seas away from the boundary current regions. The mean eddy kinetic energy (EKE) distribution map, Figure 8, computed from the 3.5-day averaged, low-passed drifter trajectories shows patterns similar to those of Figure 5, with low values in the interior of the Irminger Sea, and higher values in the boundary currents over the Reykjanes Ridge. These results are similar to those found at mid depth in the analysis of Lavender *et al.* (2000).

The mean calibrated salinity distribution computed from float data in winter (December–April) and summer (June through September) at 50 dbar, 200 dbar and 1200 dbar, Figure 9, shows for all three depth horizons and summer and winter seasons, the salinity differences between the fresher interior of the Irminger Sea and the saltier water within the cyclonic flow of the Irminger Current. A similar pattern can be seen in the distribution of potential temperatures (Fig. 10) below 200 dbar where the direct effect of wintertime surface cooling is less pronounced. These plots suggest that the southwestern Irminger Basin would be the best site for deep overturning rather than the peripheral and northeast regions.
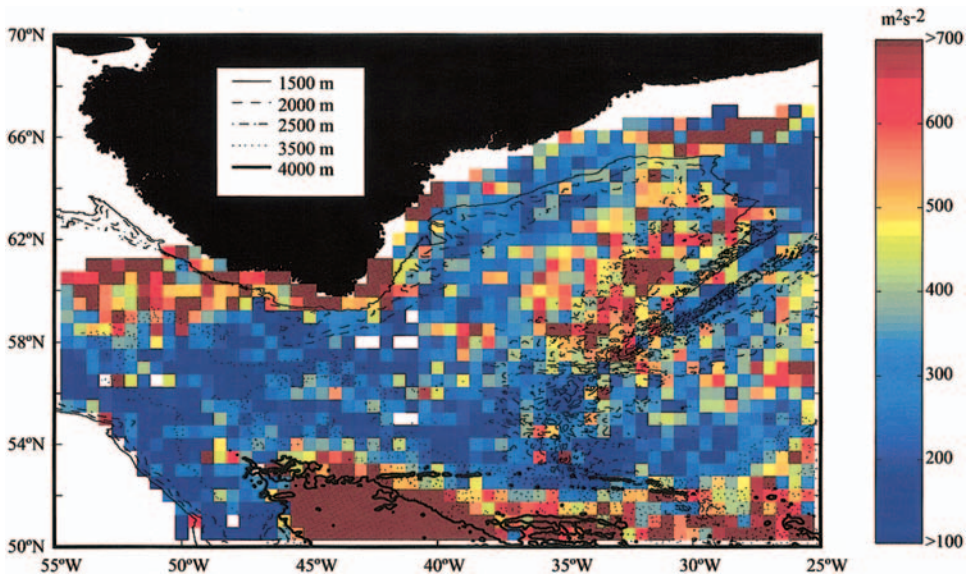
Figure 8. Eddy kinetic energy per unit mass computed from filtered drifter velocity observations with the Ekman velocity removed. The data were averaged onto a 0.5° × 0.5° grid.

The relatively weak mean surface flow there (Fig. 6), coincides with the recirculation region at 700 m discussed in the analysis of Lavender *et al.* (2002) and, therefore, reinforces this hypothesis.

Time series of the basin average potential temperature and salinity of the LSW core, defined as the cold (typically below 3.4°C) and fresh signature in the θ-*S* space, and their range (Fig. 11), show a positive trend although data are sparse between the end of WOCE (1998) and the start of Argo (2000 onwards). This trend is similar to that seen over the period up to mid 2003 at Station Bravo in the central Labrador Sea (near 57N, 62W (Ross Hendry, personal comm.).

The thermal energy per unit surface as defined by Eq. 1 (Fig. 12) shows the boundary between the warmer water of Atlantic origin and the colder water of polar origin for both the winter (January through the first week of April) and summer (June through September) seasons. In winter the region of weakly stratified water (in potential temperature) extends from the Labrador Sea into the southeastern Irminger Sea. Four profiles indicate another low energy region embedded in the warm Irminger Current southeast and east of Cape Farewell. Its separation from the central region may be an artifact of the sparse sampling. A tongue of water of high thermal energy is found at ~52.5N and between ~48W and ~43W (northwest corner region) a consequence of the recirculation at its western end, as shown by Lavender *et al.* (2000). The summer distribution shows the effect of the seasonal warming in the northeastern and peripheral Irminger Sea and is similar to the winter distribution south of Cape Farewell.
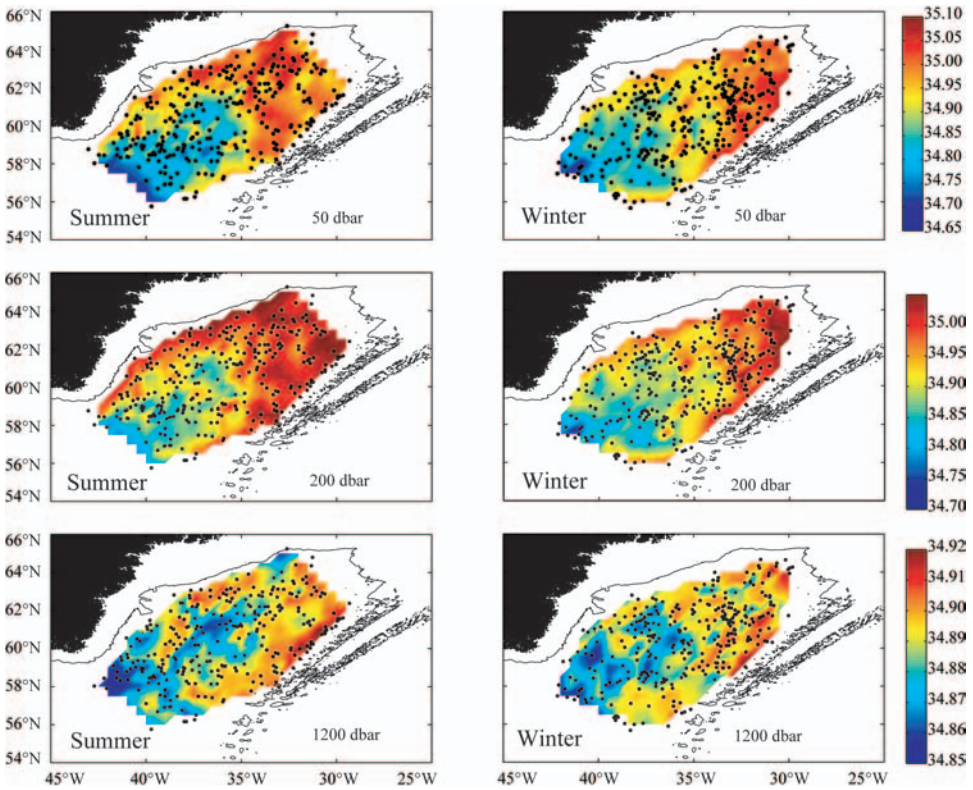
Figure 9. Salinity distribution in the Irminger Sea in summer and winter, linearly interpolated onto a 0.5° × 0.5° grid, at 50 dbar, 200 dbar and 1200 dbar. The black dots indicate the position of the float profiles. Summer is defined between June and September (and spanning between June 1997 and June 2003). Winter is defined between January and the first week of April (and spanning between January 1997 and April 2003). The black line is the 1500 m bathymetry contour.

Figure 13 shows the amount of heat loss needed to achieve a 1000 dbar deep surface mixed layer (see Section 2). This parameter has a minimum south and east of Cape Farewell that extends westward into the Labrador Sea. The mean profiles of θ (Fig. 14) and S (Fig. 15) for winter and summer months computed from floats CTD measurements in the southwestern Irminger Sea (the region contained in the dashed rectangle of Fig. 13) are also shown together with their yearly cycle at selected depths. The strong seasonal cycle is apparent from these plots and the vertical homogenization of salinity in winter months near values typical of the LSW core, to a certain extent analogous to the one observed in the Labrador Sea (Lilly *et al.,* 1999; Steffen and D'Asaro, 2002), indicate convecting activity.

4. Discussion and conclusions

The CTD profiles measured by autonomous profiling floats in the last decade have provided a basis for observing the mean wintertime conditions of the upper water
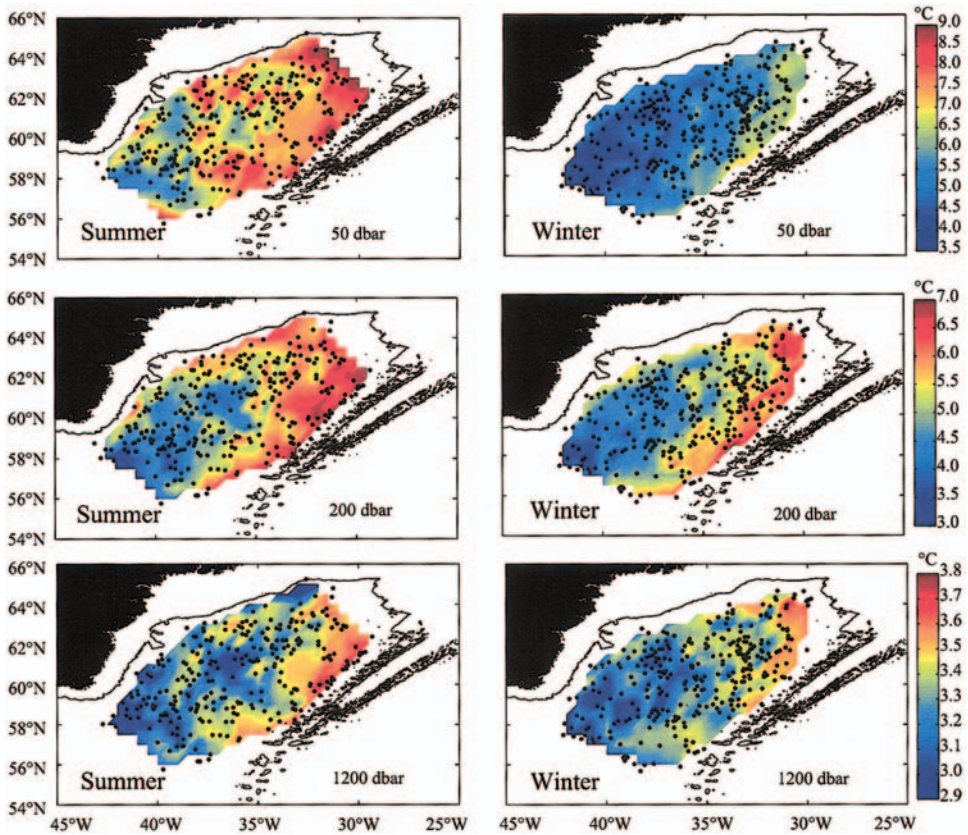
Figure 10. As Figure 9 but for potential temperature.

masses in the Irminger Sea. In summer, at the southwestern end of the Irminger Sea and away from the Irminger Current region, the upper part of the ocean is subject to positive buoyancy fluxes that produce water much warmer and fresher than in winter months (Figs. 14 and 15). Under intense winter cooling, the surface layer can sometimes cool to temperatures close to (or even below) those of the LSW core and still be statically stable because of the compensating effect of low salinities (not shown but see, for example, Steffen and D'Asaro (2002) for a discussion of similar winter profiles in the contiguous Labrador Sea). Therefore, if one wants to model the deepening of the mixed layer and estimate its maximum depth, temperature profiles used as proxies for density are inadequate as they would systematically lead to an overestimate of the mixing depth. Instead, density profiles must be used. Following Pickart *et al.* (2003a), and based on the results of Figure 13 which allows us to focus on the region where deep convection is most likely to occur, we now wish to estimate the depth of the surface mixed layer at the end of March by applying a heat flux that
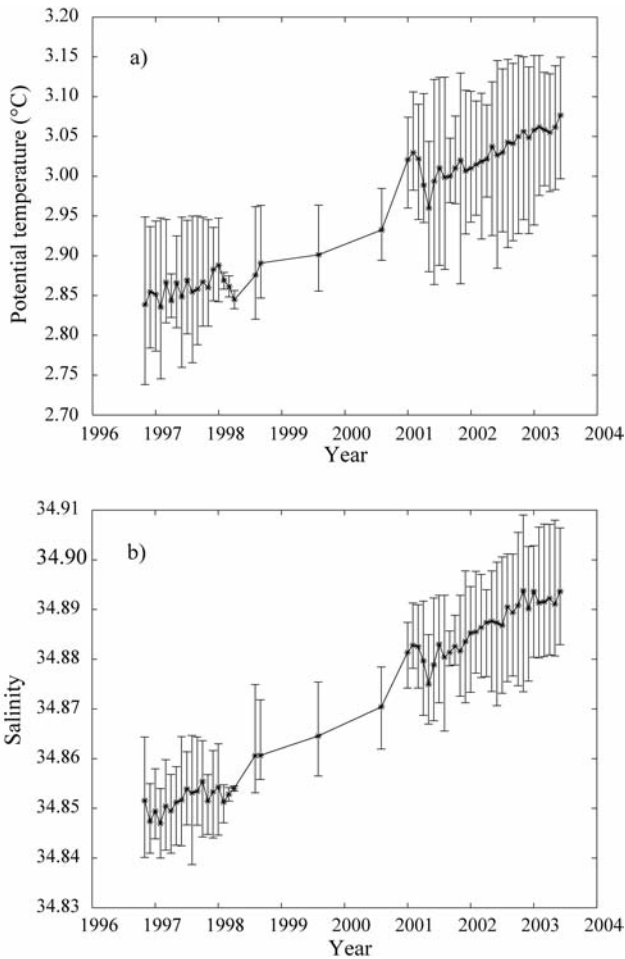
Figure 11. Potential temperature and salinity time series of LSW averaged inside the Irminger Sea (that is, inside the region bounded by the dashed rectangle in Fig. 3). The error bars denote the range (minimum and maximum values).

simulates the Greenland tip jet. A one-dimensional mixed layer model is appropriate in regions such as near the center of the upward-domed isopycnals region of the Irminger Sea, where the mean flow and the eddy kinetic energy are weak. Such a region is also favorable to preconditioning, a term used to define the weakening of the stratification by buoyancy fluxes before deep convection can occur (e.g. Pickart *et al.,* 2003b). From the θ and *S* measurements taken in the southwestern Irminger Sea (dashed box in Fig. 13) we ran three different one-dimensional mixed layer models. The first model describes rotating convection (Niiler and Krauss, 1977; Wang, 2003) and uses a linear equation of state. The governing equations are:
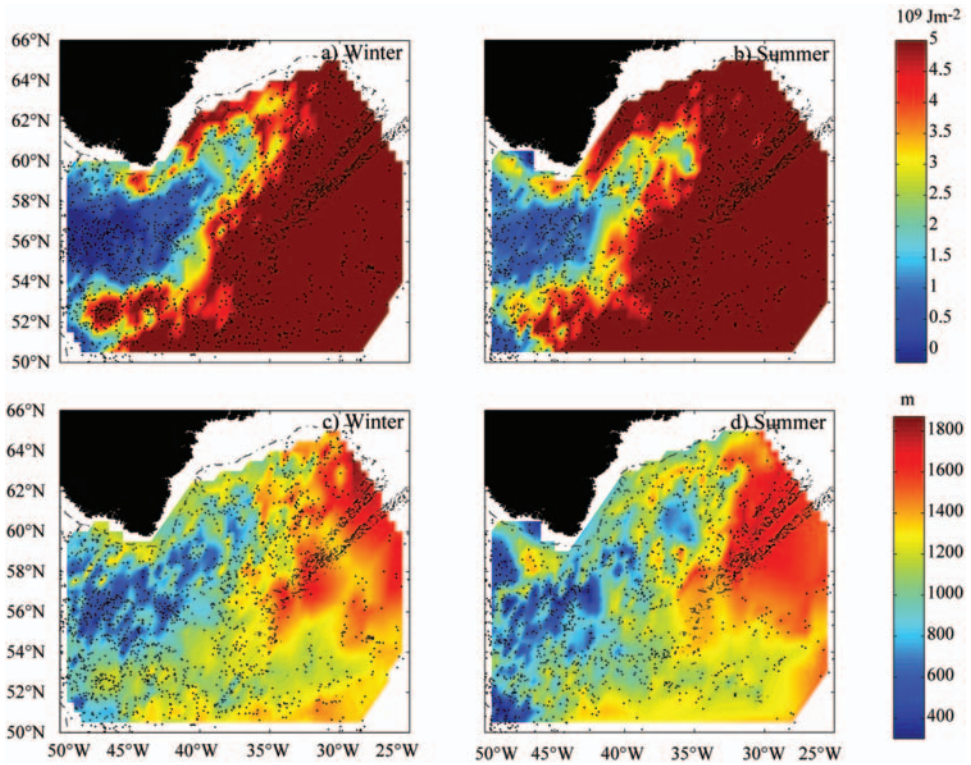
Figure 12. Thermal energy per unit area computed with Eq. 1 for winter (a) January through the first week of April and summer (b) June through September and the depth of the ~3.3°C isotherm for winter (c) and summer (d). The dots indicate the position of the float CTD profiles. The black dash-dotted lines indicate the 1500 depth contour.

$$\frac{dh}{dt} = n\,\frac{B_0}{\Delta b}, \tag{2a}$$

$$h\,\frac{db}{dt} = (1-n)B_0, \tag{2b}$$

$$n = 0.2\,\tanh\,(R_0^{1/2}), \tag{2c}$$

$$R_0 = \frac{(B_0/f)^{1/2}}{f/h}. \tag{2d}$$

Here h is the depth of the surface mixed layer, B_0 is the surface buoyancy flux, negative when heat is lost to the atmosphere, Δb is the buoyancy jump at the base of the mixed layer, b is the buoyancy of the mixed layer, R_0 is the Rossby number and f is the Coriolis parameter. The entrainment of water at the base of the mixed layer is
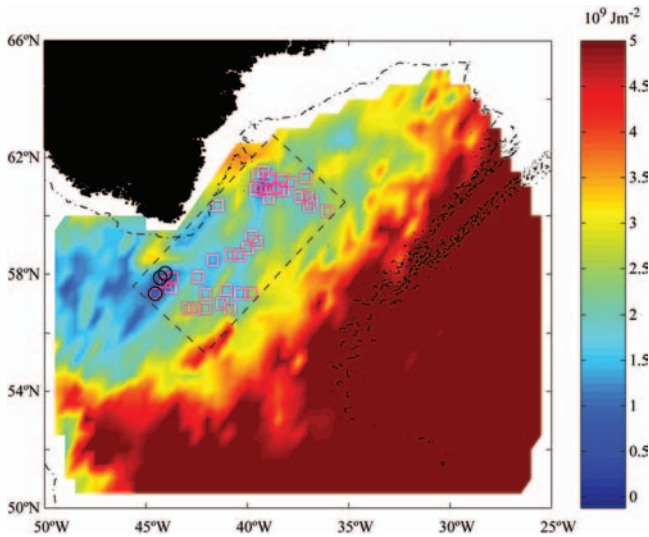
Figure 13. Heat loss needed to create 1000 dbar deep mixed layers. The dashed rectangle bounds the region inside which the mixed layer depth at the end of March was computed, from measured profiles, by applying three different 1-D models and the locations of computed values greater than 800 dbar are marked with squares. Black circles mark the position of observed mixed layer depths greater than 800 dbar (between the last week of March and the first week of April).

parameterized by n in Eq. 2a. In the nonrotating limit, as $f \rightarrow 0$, $n \rightarrow 0.2$ (e.g. Wang, 2003). The second model describes rotating convection with a nonlinear equation of state, and therefore Eqs. 2a, 2c and 2d hold, while Eq. 2b must be substituted by the heat and salt equations

$$\frac{dS}{dt} + \frac{\Delta S}{h}\frac{dh}{dt} = 0$$

$$\frac{d\theta}{dt} + \frac{\Delta\theta}{h}\frac{dh}{dt} = \frac{Q_0}{\rho c h}$$

(3)

from which the buoyancy of the mixed layer is recomputed using the nonlinear equation of state. In Eq. 3, θ and S are the potential temperature and the salinity of the mixed layer, ΔS and $\Delta\theta$ are, respectively, the salinity and the potential temperature jump at the base of the mixed layer, Q_0 is surface heat flux, ρ is the water density and c is the specific heat. The third model, already mentioned in Section 2 and used to produce Figure 13, for each time step and given the prescribed buoyancy flux, lowers the temperature of the mixed layer and deepens it until the water column is statically stable (Clarke and Gascard, 1983). For all models, the heat loss associated with the Greenland tip jet (Pickart *et al.,* 2003a) was simulated by using a buoyancy flux in the
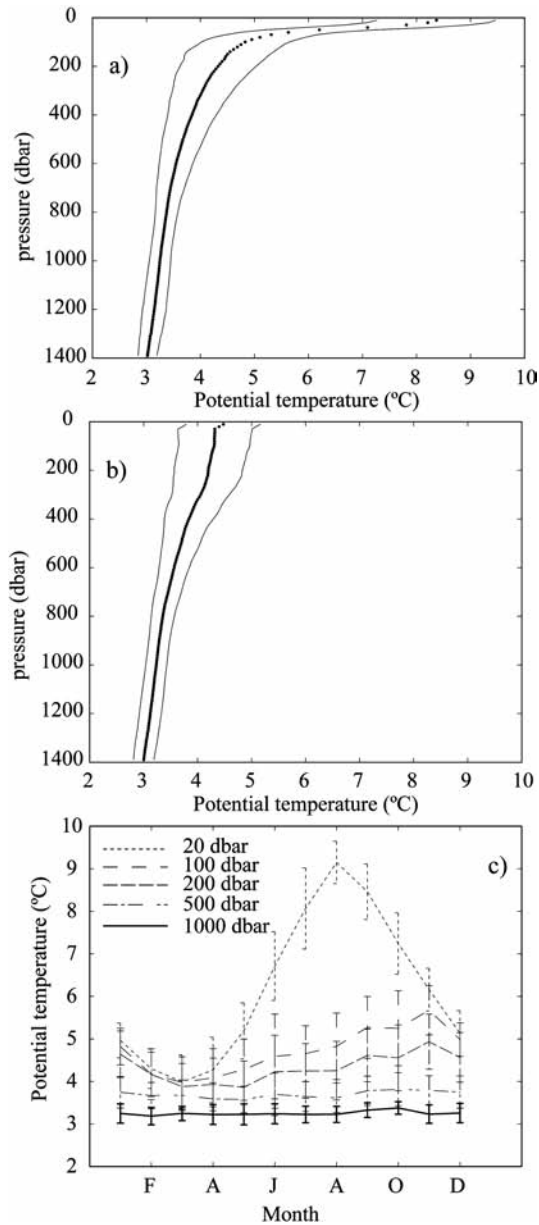
Figure 14. Mean potential temperature profile (thick line) and standard deviation (thin line) for summer (a) June through September and winter (b) January through the first week of April computed from the Irminger Sea float profiles located in the region for which the 1-D mixed layer models were run. This region is shown in Figure 13. Time series (c) computed from the same profiles at selected depth.
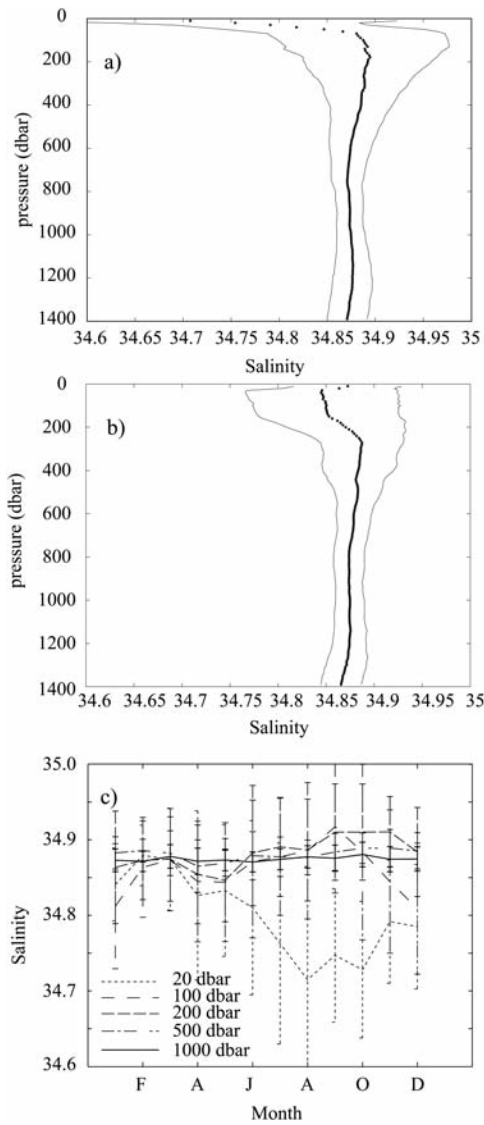
Figure 15. As Figure 14 but for salinity.

form of a periodic square wave with a 13 day period, 3-day wide peaks of $-12.5 \ 10^{-8} \ \mathrm{m^2 \ s^{-3}}$ and a value of $-3.7 \ 10^{-8} \ \mathrm{m^3 \ s^{-2}}$ elsewhere, corresponding, if evaporation is neglected (Lilly *et al.,* 1999), to net heat fluxes of about 500 W m^{-2} and 140 W m^{-2}. The buoyancy forcing was applied to the float profiles from their acquisition date to the end of March. Figure 16 shows the frequency of occurrence of the mixed layer depths computed with the three models together with frequency of
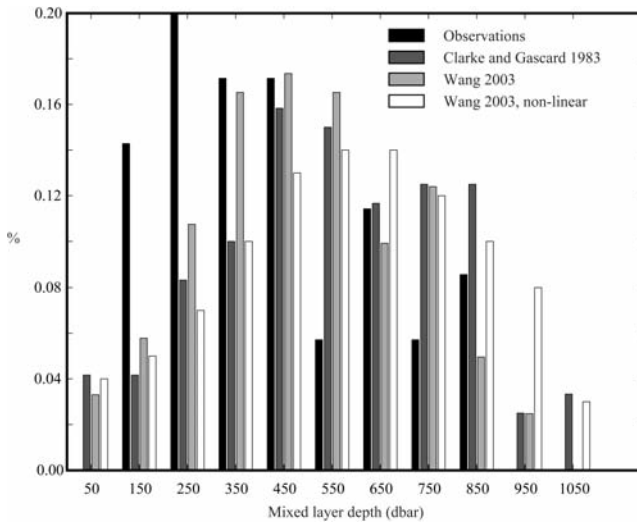
Figure 16. Frequency of occurrence of modeled and observed mixed layer depths inside the dashed
rectangle in Figure 13.

occurrence of the observed values, in the same area, during the last week of March and
the first week of April (the mixed layer depth of the measured profiles was estimated by
visual inspection, and corresponded to a lower limit at the top of the sharp interface
separating the stratified lower part of the cast from the upper homogeneous one). The
mean values of the distributions are: 489 dbar for linear rotating convection, 571 dbar
for nonlinear rotating convection and 550 dbar for the Clarke and Gascard (1983)
model. All these figures are consistent amongst themselves and slightly larger than a
mean observed mixed layer depth of 424 dbar. In our model calculation we assume that
restratification by lateral eddy fluxes is negligible and, therefore, water masses with
uniform θ and S should remain so for a few weeks after the convective activity reaches
its maximum strength in March. The predicted mixed layer depth computed with these
models is two to four times smaller than estimates obtained with regional oceanic
models (Pickart *et al.,* 2003a). The difference in initial conditions (Pickart *et al.*
(2003a) used casts from a late summer cruise from a high NAO year) may partly
explain the discrepancy. Predicted and observed mixed layer depths greater than
800 dbar are shown in Figure 13. These modeled and observed mixed layer estimates
should be interpreted with caution since the sampling achieved with Lagrangian floats
profiling only every ten days or so is not well suited to investigate highly localized
convective events with an aspect ratio of about one and possibly associated with water
masses with homogeneous θ and S over horizontal scales of $\sim$10 km (Clarke and
Gascard, 1983). Furthermore, more realistic heat fluxes could significantly modify the
modeled results. Nevertheless, profiling floats sample the differences in the mean
properties between areas where deep convection is known to occur and areas where it

is not. For example, Lavender *et al.* (2000, 2002) have found that the mixed layer depth in the Irminger Sea for the winters between 1996 and 1998 is typically shallower than 400 m, which contrasts with the much larger values recorded at the LSW formation site in the Labrador Sea at the same time.

The analyzed data cannot discern whether the observed and the modeled mixed layer depths represent a preferred state or whether we are just observing a period with lower than average winter heat fluxes or for which the surface layer in the southwestern Irminger Sea is too buoyant (either being too fresh and/or too warm) to be convected to greater depths. The warming and increasing salinity trend, captured by the float array and shown in Figure 11 (see also Pickart *et al.* (2003b) for similar plots reaching mid-1997, and for example, Dickson *et al.* (1996), for an analysis in the Labrador Sea), is perhaps the best proof that a significant production of LSW is unlikely to have taken place, in the period examined, south and southwest of Cape Farewell. This conclusion is reinforced by similar simultaneous observations in the Labrador Sea.

APPENDIX

Table 1. List of WMO ID of the Argo floats used in this study. The pre-Argo floats are not listed in this table and are available from the WOCE Global Data Version 3.0 (WOCE Data Products Committee, 2002).

15855	49068	62742	64677	4900298	6900157	6900198
41534	62677	62743	64678	4900299	6900158	6900199
44745	62678	62744	64681	4900300	6900161	
44747	62683	62746	64683	6900082	6900173	
44750	62687	62747	64685	6900083	6900174	
44870	62688	62748	4900190	6900084	6900175	
49064	62689	62749	4900222	6900086	6900183	
49065	62690	64596	4900223	6900154	6900185	
49066	62735	64598	4900224	6900155	6900186	
49067	62738	64671	4900225	6900156	6900197	

Table 2. List of cruises from which CTD data were used to calibrate the salinity data from floats. Earlier cruises not listed are available from the WOCE Global Data Version 3.0 (WOCE Data Products Committee, 2002).

Vessel	Cruise	Date	PI
Oceanus	369	2–27 Aug. 2001	R. Pickart
Meteor	45/4	13–32 Aug. 1999	J. Meincke
Meteor	50/3	21 June–15 July 2001	J. Holfort
Poseidon	263	2–28 Aug. 2000	U. Huebner
Poseidon	290	6–24 June 2002	J. Holfort
Valdivia	173	15 Aug.–1 Sept. 1998	K. Schultze
Discovery	258	1 Nov.–18 Dec. 2001	R. Pollard and S. Hay
Discovery	262	18 Apr.–27 May 2002	K. Richards
Discovery	264	25 Jul.–28 Aug. 2002	A. Brierly
Discovery	267	6 Nov.–18 Dec. 2002	J. Allen and S. Hay

REFERENCES

Bacon, S., L. R. Centurioni and W. J. Gould. 2001. The evaluation of salinity measurements from PALACE floats. J. Atmos. Oceanic Tech., *18,* 1258–1266.

Bacon, S., G. Reverdin, I. G. Rigor and H. M. Snaith. 2002. A freshwater jet on the east Greenland shelf. J. Geophys. Res., *107*(C7), 5.1–5.16, 3068, doi:10.1029/2001JC000935.

Bersch, M., J. Meincke and A. Sy. 1999. Interannual thermohaline changes in the northern North Atlantic 1991–1996. Deep-Sea Res. II, *46,* 55–75.

Bruce, J. G. 1995. Eddies southwest of the Denmark Strait. Deep-Sea Res. I, *42,* 13–29.

Clarke, R. A. and J. Gascard. 1983. The formation of Labrador Sea water. Part I: Large-scale processes. J. Phys. Oceanogr., *13,* 1764–1778.

Davis, R. 1998. Autonomous floats in WOCE. Int. WOCE Newsletter, *30,* 3–6.

Davis, R., D. C. Webb, L. A. Regier and J. Dufour. 1992. The Autonomous Lagrangian Circulation Explorer (ALACE). J. Atmos. Oceanic Tech., *9,* 264–285.

Dickson, R. R., E. M. Gmitrowicz and A. J. Watson. 1990. Deep-water renewal in the northern North Atlantic. Nature, *344,* 848–850.

Dickson, R., J. Lazier, J. Meincke, P. Rhines and J. Swift. 1996. Long term coordinated changes in the convective activity of the North Atlantic. Progr. Oceanogr., *38,* 241–295.

Doyle, J. D. and M. A. Shapiro. 1999. Flow response to large-scale topography: the Greenland tip jet. Tellus, *51A,* 728–748.

Eden, C. and C. Böning. 2002. Sources of eddy kinetic energy in the Labrador Sea. J. Phys. Oceanogr., *32,* 3346–3363.

Fratantoni, D. M. 2001. North Atlantic surface circulation during the 1990's observed with satellite-tracked drifter. J. Geophys. Res., *106,* 22067–22094.

Katsman, C. A., M. A. Spall and R. S. Pickart. 2004. Boundary current eddies and their role in the restratification of the Labrador Sea. J. Phys. Oceanogr. (in press).

Krauss, W. 1995. Currents and mixing in the Irminger Sea and in the Iceland Basin. J. Geophys. Res., *100*(C6), 10851–10872.

——— 1996. A note on overflow eddies. Deep-Sea Res. I, *43,* 1661–1667.

Lavender, K. L., R. E. Davis and W. B. Owens. 2000. Mid-depth recirculation observed in the interior Labrador and Irminger seas by direct velocity measurements. Nature, *407,* 66–69.

—— 2002. Observations of open-ocean deep convection in the Labrador Sea from subsurface floats. J. Phys. Oceanogr., *32,* 511–526.

Lilly, J. M., P. B. Rhines, M. Visbeck, R. Davis, J. R. N. Lazier, F. Schott and D. Farmer. 1999. Observing deep convection in the Labrador Sea during winter 1994/1995. J. Phys. Oceanogr., *29,* 2065–2098.

Mortensen, J. and H. Valdimarsson. 1999. Thermohaline changes in the Irminger Sea, ICES CM 1999/L:16, 11 pp (unpublished manuscript).

Niiler, P. P. 2001. The World Ocean surface circulation, *in* Ocean Circulation and Climate— Observing and Modeling the Global Ocean, G. Siedler, J. Church and J. Gould, eds., Academic, San Diego, CA, 640 pp.

Niiler, P. P. and E. B. Krauss. 1977. One-dimensional models of the upper ocean, *in* Modelling and Prediction of the Upper Layers of the Ocean, E. B. Krauss, ed., Pergamon, NY, 325 pp.

Niiler, P. P., N. A. Maximenko, G. G. Panteleev, T. Yamagata and D. B. Olson. 2003. Near-surface dynamical structure of the Kuroshio Extension. J. Geophys. Res., *108,* C6, 24.1–24.19, doi:10.1029/2002JC001461.

Orvik, K. A. and P. P. Niiler. 2002. Major pathways of Atlantic water in the northern North Atlantic and Nordic seas toward Arctic. Geophys. Res. Lett., *29,* 19, 2.1–2.4, doi:101029/2002GL015002.

Pickart, R. S., M. A. Spall, M. H. Ribergaard, G. W. K. Moore and R. F. Milliff. 2003a. Deep convection in the Irminger Sea forced by the Greenland tip jet. Nature, *424,* 152–156.

Pickart, R. S., F. Straneo and G. W. K. Moore. 2003b. Is Labrador Sea water formed in the Irminger Basin? Deep-Sea Res. I, *50,* 23–52.

Ralph, E. and P. P. Niiler. 1999. Wind-driven currents in the tropical Pacific. J. Phys. Oceanogr., *29,* 2121–2129.

Reverdin, G., P. P. Niiler and H. Valdimarsson. 2003. North Atlantic Ocean surface currents. J. Geophys. Res., *108,* C1, 2.1–2.21, doi: 10.1029/2001JC001020.

Roemmich, D., H. Freeland, K. Kim, B. King, R. Molinari, W. B. Owens, S. Riser, U. Send and P. Y. Le Traon. 2001. Argo: the global array of profiling floats, *in* Observing the Oceans in the 21st Century, K. J. Koblinsky and N. R. Smith, eds., GODAE Project Office and Bureau of Meteorology, Melbourne, 604 pp.

Rudels, B., E. Fahrbach and J. Meincke. 1999. The East Greenland Current form Fram Strait to beyond Denmark Strait in 1998: observations from RV *Polarstern* and RV *Valdivia.* ICES CM 1999/L:23, 20 pp. (unpublished manuscript).

Smith, W. H. F. and D. T. Sandwell. 1997. Global seafloor topography from satellite altimetry and ship depth soundings. Science, *277,* 1956–1962.

Spall, M. A. and R. S. Pickart. 2003. Wind-driven recirculations and exchange in the Labrador and Irminger seas. J. Phys. Oceanogr., *33,* 1829–1845.

Steffen, E. L. and E. A. D'Asaro. 2002. Deep convection in the Labrador Sea as observed by Lagrangian floats. J. Phys. Oceanogr., *32,* 475–492.

Straneo, F., R. S. Pickart and K. Lavender. 2003. Spreading of Labrador Sea water: an advective-diffusive study based on Lagrangian data. Deep-Sea Res. I, *50,* 701–719.

Sverdrup, H. U., M. W. Johnson and R. H. Fleming. 1942. The Oceans: Their Physics, Chemistry and General Biology, Prentice-Hall, NY, 1087 pp.

Sy, A., M. Rhein, J. R. N. Lazier, K. P. Koltermann, J. Meincke, A. Putzkal and M. Bersch. 1997. Surprisingly rapid spreading of newly formed intermediate waters across the North Atlantic Ocean. Nature, *386,* 675–679.

Talley, L. D. and M. S. McCartney. 1982. Distribution and circulation of Labrador Sea water. J. Phys. Oceanogr., *12,* 1189–1205.

Wang, D. 2003. Entrainment laws and a bulk mixed layer model of rotating convection derived from large-eddy simulations. Geophys. Res. Lett., *30,* 18, 1929 doi:10.1029/2003GL017869.

WOCE Data Product Committee. 2002. WOCE Global DATA, Version 3.0. WOCE International Project Office. WOCE Report No. 180/02, Southampton, UK.

Wong, A. P. S., G. C. Johnson and W. B. Owens. 2003. Delayed-mode calibration of autonomous CTD profiling float salinity data by θ-S climatology. J. Atmos. Ocean. Tech., *20,* 308–318.

Zhang, H., M. D. Prater and T. Rossby. 2001. Isopycnal lagrangian statistics from the North Atlantic Current from RAFOS float observations. J. Geophys. Res., *106*(C7), 13817–13836.